

The nature of assembly bias - III. Observational properties

Ivan Lacerna¹, Nelson Padilla^{2,3} and Federico Stasyszyn^{4,5}

¹*Instituto de Astronomía, Universidad Nacional Autónoma de México, A. P. 70-264, 04510, México, D.F., México*

²*Instituto de Astrofísica, Pontificia Universidad Católica de Chile, Av. V. Mackenna 4860, Santiago, Chile*

³*Centro de Astro-Ingeniería, Pontificia Universidad Católica de Chile, Av. V. Mackenna 4860, Santiago, Chile*

⁴*Leibniz-Institut für Astrophysik Potsdam (AIP), An der Sternwarte 16, Postdam, Germany*

⁵*Universitäts Sternwarte München, Scheinerstr. 1, D-81679 München, Germany*

ABSTRACT

We analyse galaxies in groups in the Sloan Digital Sky Survey (SDSS) and find a weak but significant assembly-type bias, where old central galaxies have a higher clustering amplitude (61 ± 9 per cent) at scales $> 1 h^{-1}$ Mpc than young central galaxies of equal host halo mass ($M_h \sim 10^{11.8} h^{-1} M_\odot$). The observational sample is volume-limited out to $z = 0.1$ with $M_r - 5 \log(h) \leq -19.6$. We construct a mock catalogue of galaxies that shows a similar signal of assembly bias (46 ± 9 per cent) at the same halo mass. We then adapt the model presented by Lacerna & Padilla (Paper I) to redefine the overdensity peak height, which traces the assembly bias such that galaxies in equal density peaks show the same clustering regardless of their stellar age, but this time using observational features such as a flux limit. The proxy for peak height, which is proposed as a better alternative than the virial mass, consists in the total mass given by the mass of neighbour host haloes in cylinders centred at each central galaxy. The radius of the cylinder is parametrized as a function of stellar age and virial mass. The best-fitting sets of parameters that make the assembly bias signal lower than 5–15 per cent for both SDSS and mock central galaxies are similar. The idea behind the parametrization is not to minimize the bias, but it is to use this method to understand the physical features that produce the assembly bias effect. Even though the tracers of the density field used here differ significantly from those used in Paper I, our analysis of the simulated catalogue indicates that the different tracers produce correlated proxies, and therefore the reason behind this assembly bias is the crowding of peaks in both simulations and the SDSS.

Key words: galaxies: formation - galaxies: haloes - galaxies: statistics - cosmology: dark matter - cosmology: large-scale structure of Universe.

1 INTRODUCTION

In current hierarchical clustering models, galaxies form by gas cooling inside virialized cold dark matter haloes in a way that makes their properties depend only on the halo mass in which they form. In the last few years, results from N -body simulations have shown that the halo clustering at large-scales depends on other halo properties in addition to the halo mass (e.g. Gao et al. 2005; Wechsler et al. 2006; Zhu et al. 2006; Gao & White 2007; Faltenbacher & White 2010; Lacerna & Padilla 2011, 2012; van Daalen et al. 2012). This effect in haloes, that is not expected from the excursion set theory, was termed ‘assembly bias’. For example, low-mass haloes assembled at high redshifts are more strongly correlated than those of the same mass assembled more recently. Therefore, one could ask whether the assembly bias could affect the assumption

that galaxy properties, e.g. galaxy clustering, depend only on the host halo mass.

By means of a semi-analytic model of galaxy formation, Croton et al. (2007) showed that galaxy clustering on large scales is affected by the correlation of halo environment with halo assembly history. Lacerna & Padilla (2011, hereafter Paper I) found an assembly bias effect in the semi-analytic galaxies from the Lagos et al. (2008) model, where the old population has a higher clustering at large scales than the young population with the same host halo mass. Using semi-analytic models, Xie et al. (2014) found that the assembly bias may result in an abundance fraction 25 per cent lower for void galaxies than the expected by using their stellar-to-halo mass relation.

On the observational side, the existence of the assembly bias is still debated. For example, Skibba et al. (2006, see also Skibba & Sheth 2009) used galaxies from the Sloan Digital Sky Survey (SDSS; York et al. 2000) to measure marked

arXiv:1110.6174v5 [astro-ph.CO] 3 Jul 2014

correlation functions that when analysed using the halo model suggest that the correlation between halo formation and environment is not important for the bright galaxy population. Tinker et al. (2011) found similar results, indicating that this dependence arises just from the correlation between halo mass function and environment. However, Yang et al. (2006) and Wang et al. (2008) found that groups with red central galaxies, selected from the Two Degree Field Galaxy Redshift Survey (2dFGRS; Colless et al. 2001) and SDSS respectively, are more strongly clustered than groups of the same mass but with blue central galaxies, this effect being much more important for less massive groups. Zapata et al. (2009) found that SDSS galaxy groups of similar mass and different assembly histories show differences in their fraction of red galaxies. Furthermore, Cooper et al. (2010) studied the relationship between the local environment and properties of galaxies in the red sequence. After removing the dependence of the average overdensity on colour and stellar mass by setting a density parameter as an estimator of environment independent of these galaxy properties, they still found that galaxies with older stellar populations occupy regions of higher overdensities compared to younger galaxies of similar colours or stellar masses. Also, Alonso et al. (2012) show that galaxies in groups in low global densities are prone to show higher star formation compared to galaxies of equal properties and similar host groups but in high density environments. Recently, Wang et al. (2013b) have claimed the direct detection of the assembly bias in observations. They found that SDSS central galaxies with low specific star formation rates (sSFR) cluster more than those with high sSFR in low stellar mass bins. These results, from models and observations, show that the concept of assembly bias is applicable to galaxies in addition to dark matter (DM) haloes and would then influence the physics of galaxy formation.

The assembly bias effect is important when galaxies are used to constrain cosmological parameters. Wu et al. (2008) showed that upcoming photometric catalogues such as the Dark Energy Survey (DES)¹ and the Large Synoptic Survey Telescope (LSST; LSST Science Collaborations et al. 2009)² can infer significantly biased cosmological parameters from the observed clustering amplitude of galaxy clusters if the assembly bias is not taken into account. Furthermore, the halo-galaxy connection inferred by models using galaxy clustering and assuming only halo mass dependence, such as the halo occupation distribution (HOD, Berlind & Weinberg 2002) and the conditional luminosity function (Yang et al. 2003), can be subject to an additional systematic error due to the assembly bias (Wang et al. 2013a; Zentner et al. 2013). Hearin et al. (2014) showed that an assembly bias effect in HOD models is required for producing the signal of galactic conformity on Mpc scales, i.e. quenched central galaxies tend to reside preferentially in quenched large-scale environments (Kauffmann et al. 2013). Therefore, some properties of central galaxies such as the quenching do not depend on the halo mass alone.

Paper I presented a new peak height definition different from the halo virial mass, where semi-analytic galaxies

in haloes of a given mass but different age do not show the assembly bias effect in the two-halo regime. This new definition simply adds mass to that of the dark matter halo in a way that makes old, low-mass haloes suffer the most extreme peak height change with respect to what results of using the virial mass as its proxy. In this paper we will test this model using the galaxy catalogue of Yang et al. (2007) based on SDSS. However, instead of using the total underlying mass inside spheres of different radii, we will use the total mass of haloes inside cylinders along the position of each central galaxy in order to make a more adequate proxy for a peak height, in a similar way to what was proposed in Paper I but applicable to real galaxy catalogues. We will discuss the implications of using discrete tracers of the density field that consider neighbour distinct haloes instead of a smooth density field.

The outline of this paper is as follows. In Section 2 we present a galaxy catalogue based on the SDSS and also a mock catalogue of galaxies. In Section 3 we measure the assembly bias effect, namely, the large-scale clustering of galaxies of a given host halo mass depends on the age, for both the SDSS and the mock central galaxies. We adopt a modified version of the model from Paper I in Section 4 using observational features. The nature of the objects considered by using the proxy of the overdensity peak height is shown in Section 5, where we discuss the implications of using discrete tracers of the density field that consider neighbour haloes instead of a smooth density field. The conclusions of our results are presented in Section 6.

Throughout this paper we use the reduced Hubble constant h , where $H_0 = 100h \text{ km s}^{-1} \text{ Mpc}^{-1}$, with the following dependences: stellar age in $h^{-1} \text{ yr}$, halo mass in $h^{-1} M_\odot$, scales (distances) in $h^{-1} \text{ Mpc}$, and absolute magnitudes in $+5 \log(h)$, unless the explicit value of h is specified.

2 DATA

2.1 SDSS galaxies

We use the galaxy group catalogue constructed by Yang et al. (2007, hereafter Y07) from the New York University Value-Added Galaxy Catalog (NYU-VAGC; Blanton et al. 2005), which is based on SDSS DR4 (Adelman-McCarthy et al. 2006). Y07 dynamically associated a dark matter halo to the galaxies by using a halo-based group finder algorithm. Each halo contains one or more galaxies out to its virial radius. The group finder consists of an iterative procedure that uses average mass-to-light ratios of groups, based on the total stellar mass (or luminosity) of all group members down to some luminosity, to assign a tentative mass to each group. Then the virial radius associated to this mass is used for updating the group membership, repeating this process until convergence is reached. The full sample consists of 369 447 galaxies with redshifts in the range $0.01 \leq z \leq 0.2$.

The Y07 group catalogue includes by construction the halo (virial) mass, M_h , even when there is only one galaxy in the halo. The group masses estimated with this method can recover on average the true halo masses, with no significant systematics (Yang et al. 2008). The available halo masses in this catalogue are based on either the ranking of the characteristic stellar mass or the ranking of the characteristic

¹ See <http://www.darkenergysurvey.org/>.

² See <http://www.lsst.org/lsst/>.

luminosity in the group. We use the halo mass based on the characteristic stellar mass, which is defined as the sum of the stellar mass of all the galaxies in the halo with $M_r - 5 \log(h) \leq -19.5$, where M_r is the absolute magnitude in the r -band. When the central galaxy (usually the most massive galaxy in the halo) is fainter than the magnitude limit of the sample, the host halo does not have a mass estimate. For this reason, the lower halo mass limit in the Y07 catalogue is $\sim 10^{11.6} h^{-1} M_\odot$. Furthermore, groups with strong survey edge effects do not have halo mass estimates regardless the luminosity of their members. The latter affects only 1.6 per cent of all Y07 groups.

We select the central galaxy as the one with the highest stellar mass in the halo. We use a volume-limited sample of central galaxies out to $z = 0.1$. At this redshift, the sample is complete down to the r -band absolute magnitude $M_r - 5 \log(h) \leq -19.6$. In addition, we identify those galaxies with estimates of the host halo mass in the Y07 catalogue and with measured luminosity-weighted ages of Gallazzi et al. (2005) since this latter parameter is essential to this work.³ There are 66,692 central galaxies with estimates of stellar age and host halo mass that satisfy our requirements of absolute magnitude and redshift.

The aim of this work is to detect the assembly bias effect in central galaxies by measuring cross-correlation functions against all the SDSS galaxies from the Y07 catalogue using $M_r - 5 \log(h) \leq -19.6$ and $0.01 \leq z \leq 0.1$ (100,244 galaxies).

2.1.1 Age parameter δ_t

As was the case in Paper I, one of the most important parameters throughout this work is the age. For SDSS galaxies, we use the luminosity-weighted age (or, simply, stellar age). To study the assembly bias in galaxies, where old objects may have a different clustering than young objects of the same mass, it is not convenient to work directly with the stellar age, for example, because this quantity correlates with the mass. For instance, older central galaxies are located, on average, in massive host haloes (see Fig. 1).

In Paper I, we presented a definition of age which is independent of the host halo mass (M_h) through the δ_t dimensionless parameter

$$\delta_{t_i} = \frac{t_i - \langle t(M_h) \rangle}{\sigma_t(M_h)}, \quad (1)$$

where for the i th galaxy, t_i is its stellar age, $\langle t(M_h) \rangle$ is the median stellar age as a function of M_h , and $\sigma_t(M_h)$ is the dispersion around the median obtained from the 10 and 90 percentiles of the distribution (error bars in Fig. 1). Then, central galaxies with positive (negative) values of δ_t correspond to old (young) populations with respect to the median distribution of stellar ages at a given host halo mass. In particular, throughout the paper we use $\delta_t > 0.5$ to select old galaxies and $\delta_t < -0.5$ to select young galaxies. The scatter in the observational stellar age can be higher than the stellar age obtained in simulated galaxies such as the

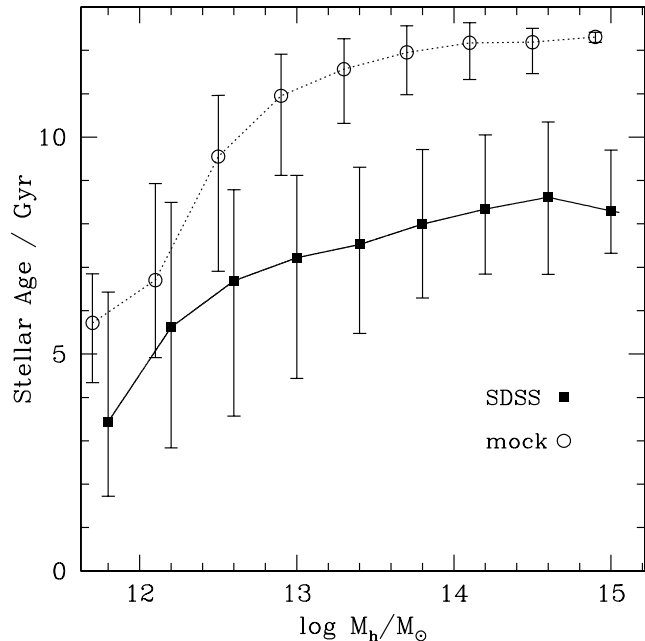


Figure 1. Median luminosity-weighted stellar age for the volume-limited sample of SDSS central galaxies (solid squares), and median mass-weighted stellar age for the volume-limited sample of mock central galaxies (open circles), as a function of the host halo mass ($h = 0.7$). Error bars correspond to the 10 and 90 percentiles of the stellar age distribution. For both samples, the median population of galaxies in low-mass haloes is younger than that of galaxies in massive haloes.

model described in Section 2.2. However, the same cuts in δ_t to select old and young galaxies are used in the SDSS and simulated samples.

2.2 The mock catalogue

We construct the mock catalogue using synthetic galaxies from the model by Lagos et al. (2008, see also Cora 2006), who combine a cosmological N -body simulation of the concordance Λ CDM universe and a semi-analytic model of galaxy formation to follow the evolution of the baryonic component of haloes across cosmic history. The numerical simulation consists in a periodic box of $150 h^{-1}$ Mpc on a side that contains 640^3 dark matter particles with a mass resolution of $\sim 10^9 h^{-1} M_\odot$. The cosmology used is $\Omega_{tot} = 1$, $\Omega_m = 0.28$ (with a baryon fraction of 0.16), $\Omega_\Lambda = 0.72$, $\sigma_8 = 0.81$, $h = 0.7$, and spectral index $n_s = 0.96$. Dark matter haloes are identified as structures that contain at least 10 particles using a friends-of-friends (FOF) algorithm (Davis et al. 1985). Another algorithm (SUBFIND; Springel et al. 2001) is applied to these groups in order to find substructures with at least 10 particles. Typically, the most massive subhalo is considered the main subhalo, while the other subhaloes are satellites within a FOF halo. The galaxy population in the semi-analytic model is generated using the merger histories of dark matter haloes and their embedded subhaloes. The virial mass for galaxies corresponds to the virial mass of their respective DM substructures.

In order to make a fair comparison between the simula-

³ Luminosity-weighted ages are obtained from <http://www.mpa-garching.mpg.de/SDSS/DR4/Data/stellarmet.html> which includes the DR4 version of the tables used in Gallazzi et al. (2005).

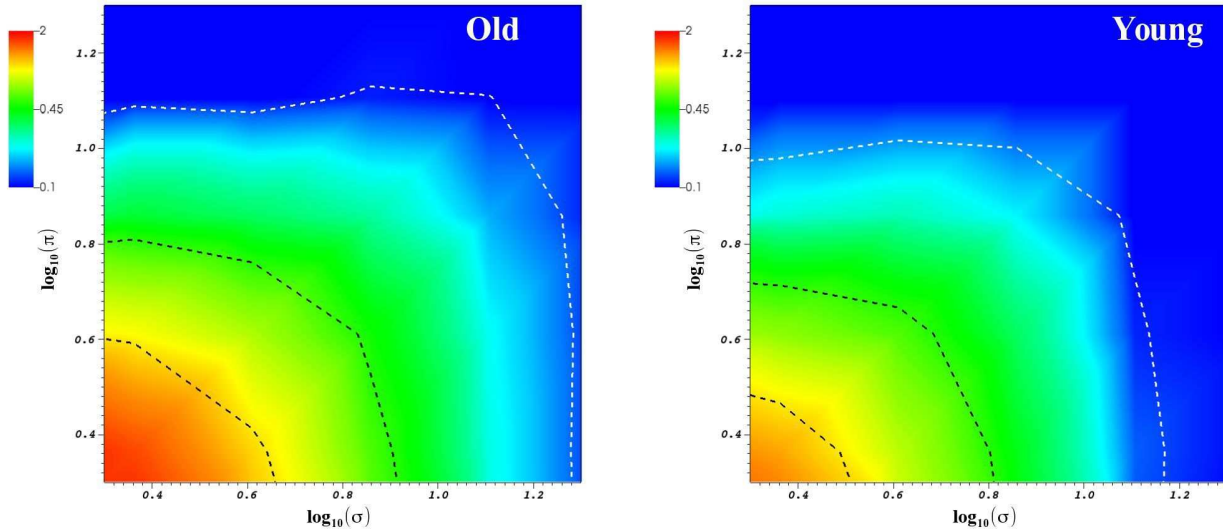


Figure 2. Cross-correlation functions in the directions parallel and perpendicular to the line of sight for old ($\delta_t > 0.5$, left panel) and young ($\delta_t < -0.5$, right panel) SDSS central galaxies in the host halo mass range $10^{11.6} < M_h/h^{-1} M_\odot < 10^{12}$. The colour in the figure key indicates the amplitude of the correlation function. The three contour levels, from large to small separations, correspond to $\xi(\sigma, \pi) = 0.1, 0.5$ and 1.0 , respectively.

tion and observations, we construct a mock SDSS catalogue using the semi-analytic galaxies. To do this we place an observer at the position $x, y, z = 0$ in the simulation box, and record the positions, peculiar velocities, apparent and absolute magnitudes (at a fixed $z = 0$ rest-frame), mass-weighted stellar ages among other properties, for galaxies whose angular positions lie within the observing mask of the SDSS DR4. The apparent magnitudes are calculated using the comoving distance to each galaxy; we apply an upper limit in magnitudes at $r = 17.77$ to mimic the selection function of the galaxy sample. We calculate redshifts taking into account both the comoving distance and the peculiar velocity projected along the line of sight, which implies our mock catalogue shows the Finger-of-God and Kaiser effects.

For the mock central galaxies, we use the virial mass of their host dark matter haloes. In general there is a good qualitative agreement between the stellar age as a function of halo mass in the mock and SDSS central galaxies (see Fig. 1). An important difference with respect to the SDSS sample is in the definition of stellar age. In the mock catalogue we use the mass-weighted stellar age in contrast to the luminosity-weighted stellar age of Gallazzi et al. (2005). For this reason, the stellar ages in the mock catalogue appear to be larger than those of the SDSS sample. The relative (normalized) age parameter δ_t is estimated for the mock central galaxies using the mass-weighted stellar age in equation (1). Using the relative age parameter ensures that using the two different age definitions does not affect our results, since these two age definitions are related via a largely one-to-one relation, even at the low age range where young stars act to further decrease the age of a galaxy.

3 ASSEMBLY BIAS IN SDSS GALAXIES

The trend that old objects are located in regions of higher densities than young objects of equal mass is readily seen in the two-point correlation function, where the ones with the higher clustering at large scales are those located on higher density regions, which could be indicating the locations of higher initial density peaks. The correlation function has the advantage that it obtains an accurate characterization of the spatial distribution of objects from kpc scales out to Mpc scales by simply measuring the excess of pairs at a given distance with respect to a random distribution. Therefore, the correlation function is a useful tool to study the large-scale environment. Our overall results will support that older populations are located in higher densities compared to younger ones at a given host halo mass.

In this section, we will test whether SDSS central galaxies show an assembly-type bias by using the two-point correlation function. Due to the redshift space distortions, we have to calculate first the cross-correlation in two coordinates $\xi(\sigma, \pi)$, where σ is perpendicular and π is parallel to the line of sight. Fig. 2 shows the resulting $\xi(\sigma, \pi)$ for the old and young central galaxies in the host halo mass range $10^{11.6} < M_h/h^{-1} M_\odot < 10^{12}$. As can be seen there is a subtle difference between both populations due to their slightly offset clustering amplitudes (c.f. Fig. 3), but also possibly due to different finger-of-god and infall effects. Given that the differences in infall are too subtle, we will not use these profiles to detect the assembly bias in contrast to Paper I.

We use the jackknife technique to estimate the variance error in the calculation of $\xi(\sigma, \pi)$, which has been shown as a robust error estimator for cosmological samples (Zehavi et al. 2002; Cabré et al. 2007), although it can overestimate the variance on small scales (Norberg et al. 2009). In general, this method consists in dividing the sample in

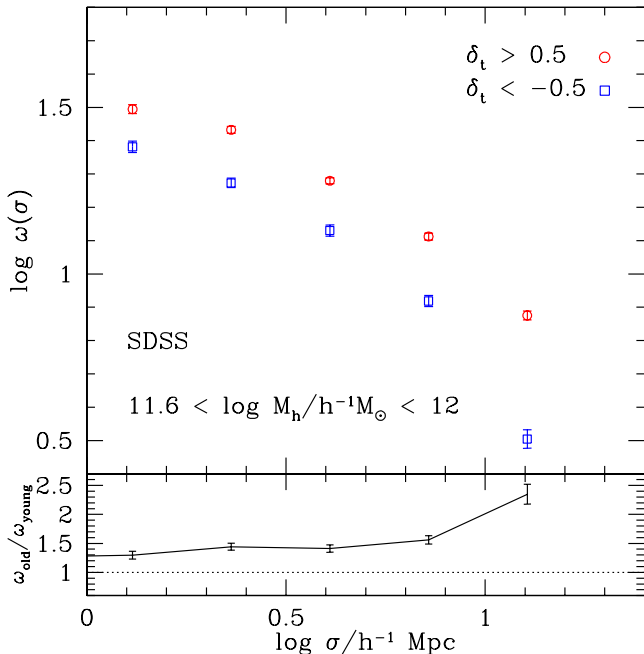


Figure 3. Projected cross-correlation functions for SDSS central galaxies. The bin in host halo mass M_h is indicated in the panel. Old and young galaxies of the same host halo mass are shown in red circles and blue squares, respectively. Error bars are calculated using the jackknife method. The lower box corresponds to the ratio between the correlation functions of the old and young populations (solid line), where the jackknife errors are taken into account. The dotted line is the unit ratio (i.e. no assembly bias).

parts and then the correlation function is calculated by discarding one of the subsamples at a time, $\xi_i(\sigma, \pi)$, and it is compared with the correlation function obtained for the whole sample $\xi(\sigma, \pi)$ as follows

$$\Delta^2 = \frac{1}{N} \sum_{i=1}^N [\xi_i(\sigma, \pi) - \xi(\sigma, \pi)]^2, \quad (2)$$

where N is the total number of subsamples. In particular, samples selected from both the SDSS and mock catalogues are divided in twenty parts, i.e. $N = 20$.

We integrate over the π component to obtain the projected correlation function $\omega(\sigma)$,

$$\omega(\sigma) = 2 \int_{\pi_{min}}^{\pi_{max}} \xi(\sigma, \pi) d\pi, \quad (3)$$

where $\pi_{min} = 0.1 h^{-1} \text{Mpc}$ and $\pi_{max} = 30 h^{-1} \text{Mpc}$. As mentioned above, we calculate projected cross-correlation functions using central galaxies. In this case, the clustering amplitude is smaller than using all the galaxies (centrals and satellites) as the main sample (see e.g. Wang et al. 2013b). Furthermore, the projected cross-correlation functions for central galaxies with halo masses larger than $10^{11.6} h^{-1} M_{\odot}$ are noisy at small scales (i.e. the one-halo term), so that we are only interested in the estimation of $\omega(\sigma)$ at large scales (i.e. the two-halo term). Fig. 3 shows $\omega(\sigma)$ for old and young SDSS central galaxies selected using limits in δ_t of equal host halo mass. We systematically find that the old galaxies show a higher clustering relative to the young population at large scales ($> 1 h^{-1} \text{Mpc}$). Therefore, SDSS central galaxies

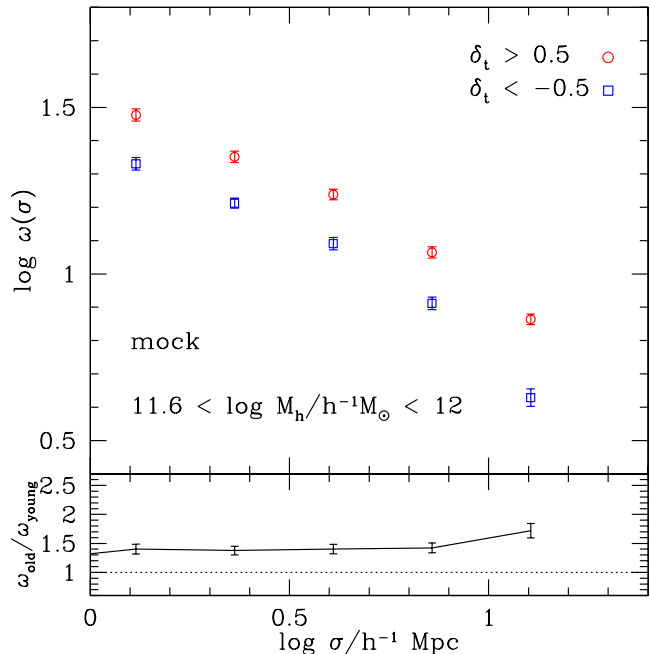


Figure 4. Same as Fig. 3 but for the mock central galaxies.

of equal host halo mass show a significant dependence of clustering amplitude with the age, i.e. the assembly bias effect with average differences of 61 ± 9 per cent for $\omega(\sigma)$.⁴ This result is in agreement with Wang et al. (2013b) who find an assembly-type bias in galaxies but using sSFR in bins of stellar mass instead of using stellar age in bins of host halo mass as done in our case. Our sample definition resembles directly those used to detect the assembly bias in simulations (see e.g. Section 3.1), and therefore constitutes a direct assembly bias measurement.

3.1 Assembly bias in the mock catalogue

Fig. 4 shows the results of the projected cross-correlation functions for the mock central galaxies hosted by haloes of the same mass as the SDSS samples. Error bars are calculated using the jackknife method. As can be seen, old mock central galaxies (red circles) are more strongly clustered than the young mock central galaxies (blue squares) in haloes of equal mass, with average differences of 46 ± 9 per cent in the clustering amplitude of $\omega(\sigma)$ at large scales ($> 1 h^{-1} \text{Mpc}$).

The results from observed SDSS central galaxies and mock central galaxies are qualitatively similar; old galaxies cluster more than young galaxies in host haloes of equal (low) mass. Quantitatively, the differences found in the clustering amplitude, i.e. the average ratio between $\omega(\sigma)$ of the old and young central galaxies, of the SDSS and mock samples are consistent with each other (e.g. bottom panels of Figs. 3 and 4). We measure a high signal of assembly bias when using $\omega(\sigma)$, which is remarkable for the SDSS central galaxies (50 – 70 per cent).

High density environments play a key role in properties

⁴ The uncertainties are estimated by using the jackknife errors.

such as the formation age. Later in this work we will use this density-age connection to obtain a peak-height proxy that traces the assembly bias effect. We will show that the crowding around objects helps us trace the assembly bias effect as efficiently as with the smooth density field approach introduced in Paper I.

4 OVERDENSITY PEAK HEIGHT PROXY USING RELATIVE AGE AND HALO MASS

In Paper I, we presented an approach to trace the assembly bias effect. This consisted in measuring the total mass inside spheres of different radii around semi-analytic galaxies, which in some cases could be larger than the virial mass of the host dark matter halo. Using two free parameters to introduce a dependence of this radius on mass and age, this model defined a new overdensity peak height for which the large-scale clustering of objects of a given mass did not depend on the age. The peak height can be thought as the size of the density perturbation that will collapse in a structure, and it is usually well represented by the virial mass; the higher the peak, the more massive will be the structure. We then analyzed the changes of this peak height proxy, compared to virial masses. We typically found that low-mass, old galaxies have larger peak heights than young galaxies of equal virial mass, which implies that the environment is more dense for old objects. They are preferentially surrounded by massive neighbour haloes, which is in agreement with other works that mention old, low-mass haloes may suffer a truncated growth due to massive neighbour haloes (Wang et al. 2007; Dalal et al. 2008; Hahn et al. 2009) or where additional effects (e.g. tidal forces) can arise in dwarf haloes ejected from massive clusters thus forming earlier than dwarf haloes in the field (Li et al. 2013). Therefore, the parametrization of the radius of the sphere to measure the environment is a useful tool to understand what is behind the assembly bias.

However, it is difficult to obtain the underlying mass information for real galaxies. For this reason, the aim of this section is to design a similar procedure, but using the host halo mass of central galaxies from Y07. The idea behind our work is not to minimize the bias, but it is to use this method to understand the physical features that produce the assembly bias.

Instead of using spheres as in Paper I, we measure the total mass inside a cylinder by considering the host halo mass of neighbour galaxies around each central galaxy along the line-of-sight to take into account the limitations imposed by the redshift space distortions. This procedure is similar to the counts-in-cylinders (e.g. Berrier et al. 2011, and more references therein), but the radius of the cylinder for each central galaxy in h^{-1} Mpc units is parametrized as

$$r = a \delta_t + b \log \left(\frac{M_h}{M_{nl}} \right), \quad (4)$$

where the free parameters are a and b , M_h is the host halo mass of the central galaxy and M_{nl} is the non-linear mass at $z = 0$.⁵ As in Paper I, we use $\log(M_{nl}/h^{-1} M_\odot) = 13.38$. (M_{nl} is a factor of normalization that only contributes to the

size of the radius r . The general results after performing the parametrization do not change when modifying the adopted value of the non-linear mass.) The length of the cylinder is $\Delta v = \pm 500 \text{ km s}^{-1}$ centred at each central galaxy.⁶ We add the halo mass of neighbour central galaxies (with masses $> 10^{11.6} h^{-1} M_\odot$ which is the lower halo mass limit in our SDSS sample) within the cylinder to obtain the total mass of distinct haloes in this volume. When the radius r is negative, the total mass of the central galaxy remains unchanged, i.e. $M = M_h$. If this radius is greater than $3 h^{-1}$ Mpc, the galaxy in the center of the cylinder will not be considered for further analysis (for the best-fitting set of parameters, none of the central galaxies in the SDSS and mock catalogues exceed this limit in radius).

Notice that this cylinder will include neighbour central galaxies and therefore this will be related to the crowding of the environment of the galaxy, a measure of the local density, but with an adaptive volume size depending on the galaxy age and host halo mass. This procedure to trace the assembly bias will use correlation functions of relatively old and young galaxies to fit the parameters of the cylinder radius, but this parametrization will only be said to correlate with the correction of Paper I (missing peak mass) if the excess of crowding in galaxies correlates with the excess of mass found in haloes reported in our previous paper. In order to demonstrate that this is the case, we first need to find the parameters that trace the assembly bias using this measurement of crowding, and then to check whether the relation between crowding and missing peak mass is present. In contrast to Paper I, we do not use the infall velocity profile because the velocity inferred from redshift space distortions is noisy compared to the velocity from numerical simulations. We apply the method first to mock galaxies and then to SDSS galaxies.

4.1 Mock galaxies

When measuring the total mass in each cylinder in the mock catalogue, we use central galaxies with $M_h > 10^{11.6} h^{-1} M_\odot$, which corresponds to the lower limit in halo mass of the SDSS sample.

We select old and young central galaxies with the relative age, δ_t , as measured in Section 2.1.1 but using the total mass M . The samples are split into three total mass bins in $\log(M/h^{-1} M_\odot)$ with the same width. For a given mass bin, the old and young subsamples contain the same number of central galaxies. The cross-correlation functions are obtained in redshift space, $\xi(\sigma, \pi)$, between the subsamples of old/young mock central galaxies against the mock sample of centrals and satellites galaxies that satisfy $M_r - 5 \log(h) \leq -19.6$ and $0.01 \leq z \leq 0.1$. We estimate their projected correlation functions as described in Section 3.

In order to find the best-fitting parameters that do not show an age dependence of the clustering, the reduced χ^2

fluctuation amplitude of the linear field is 1.69 times the critical density of the Universe, which corresponds to the gravitational collapse in the spherical collapse model.

⁶ The choice of this cylinder length corresponds to the radial velocity dispersion of poor galaxy clusters. Our general results do not change if we use other cylinder lengths, e.g. $\pm 750 \text{ km s}^{-1}$.

⁵ It is defined as the mass within a sphere for which the rms

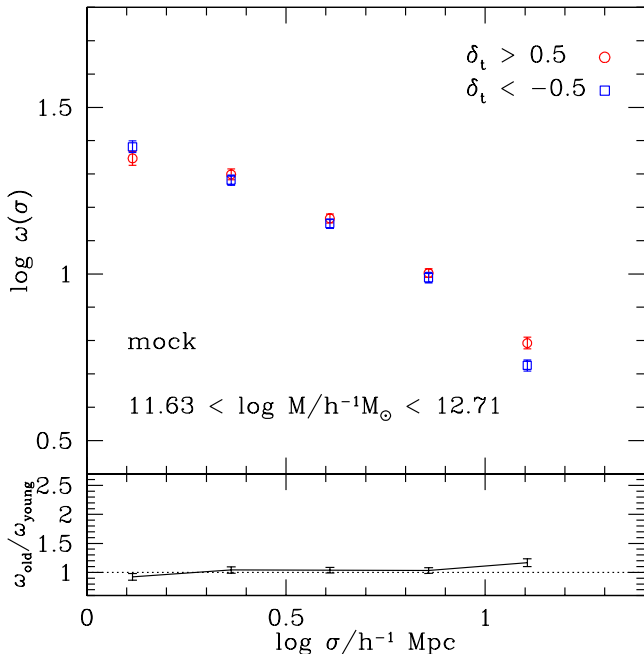


Figure 5. Projected cross-correlation functions for mock central galaxies, but with the new proxy mass M by using the best-fitting values $a = 0.3$ and $b = -0.6$ in equation (4). The mass range is indicated in the panel. Old and young mock galaxies are shown in red circles and blue squares, respectively. Error bars are calculated using the jackknife method.

for the correlation function statistics is defined as

$$\chi^2 = \frac{1}{3} \sum_i \left(\frac{1}{n_{dof}} \sum_r \frac{[\omega_{old}(\sigma) - \omega_{young}(\sigma)]^2}{\Delta_\omega^2} \right)_i, \quad (5)$$

where $\omega_{old}(\sigma)$ is the result for old galaxies and $\omega_{young}(\sigma)$ is that for young galaxies. The error is $\Delta_\omega^2 = \Delta_{\omega_{old}}^2 + \Delta_{\omega_{young}}^2$, where the first term is the jackknife error for $\omega_{old}(\sigma)$ and the second term is that for $\omega_{young}(\sigma)$. This statistics is estimated within the range $4 < r/h^{-1} \text{ Mpc} < 15$, i.e. in the two-halo term. The symbol n_{dof} denotes the number of degrees of freedom. The χ^2 value is the average over the three total mass bins.

The best-fitting parameters corresponding to the highest likelihood in the full parameter space for mock galaxies are $a = 0.3$ and $b = -0.6$ ($\chi^2 \sim 2.58$). Fig. 5 shows the cross-correlation functions of old and young mock central galaxies using these values, for the lowest mass bin of M . The assembly bias for this mass bin is on average reduced to 4 ± 6 per cent in the mock sample after using this formalism.

Fig. 6 shows an example of the method to estimate the total mass. The filled pentagon shows the position of a central galaxy with halo mass $M_h = 8.3 \times 10^{11} h^{-1} M_\odot$. The solid circle describes the radius of the cylinder around this galaxy using equation (4) with the best-fitting values $a = 0.3$ and $b = -0.6$. The solid squares show all the neighbour distinct host haloes within the cylinder. In this case, it is just one halo of mass $M_h = 7.1 \times 10^{12} h^{-1} M_\odot$. The total mass inside the cylinder, or the proxy of peak height for the central galaxy (filled pentagon), is then $M = 7.9 \times 10^{12} h^{-1} M_\odot$.

Fig. 7 shows the likelihood functions for the mock sam-

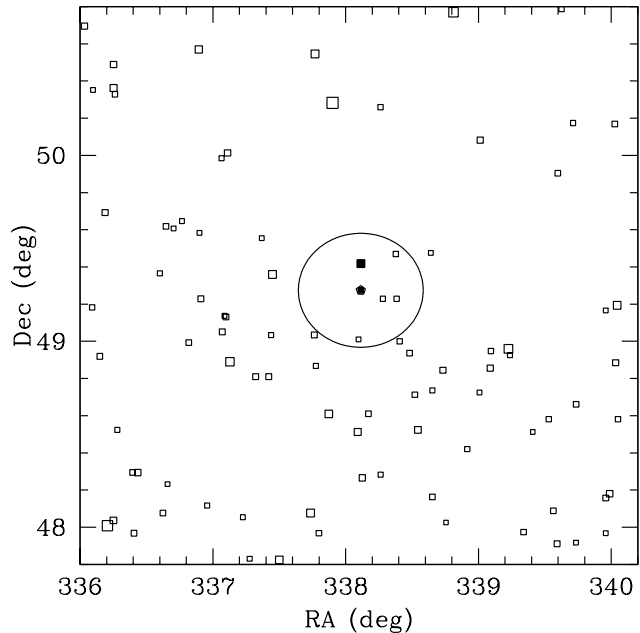


Figure 6. Distribution in Right Ascension and Declination of some distinct host haloes (squares) in the mock catalogue. The size of the squares is proportional to the halo mass. As an example of the method described in Section 4, the filled pentagon shows the position of a central galaxy. The solid circle describes the physical radius of the cylinder around this galaxy using equation (4) with the best-fitting values $a = 0.3$ and $b = -0.6$ (see Section 4.1). The length of the cylinder is $\Delta v = \pm 500 \text{ km s}^{-1}$ with respect to the central galaxy. The solid squares show all the neighbour distinct host haloes within the cylinder.

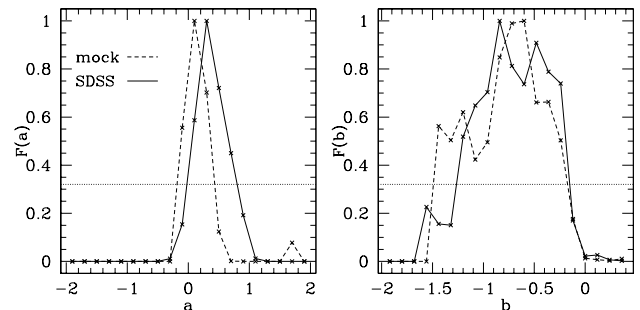


Figure 7. Marginalized likelihood functions for the free parameters a and b (left and right panels, respectively) using mock galaxies (dashed lines) and SDSS galaxies (solid lines). Both approaches for the total mass in cylinders of radius r (see equation 4) obtain roughly similar maximum values in the range of 1σ (intersection of distributions with the horizontal dotted line).

ple (dashed lines) and those of the SDSS sample (solid lines, see Section 4.2 for details). Notice that the maximum likelihood in this figure occurs for parameter values that do not necessarily coincide with those of the maximum likelihood in the full parameter space. We find that both approaches for the total mass obtain roughly similar maximum likelihood values consistent within a 1σ confidence (indicated by the intersections of the parameter distributions with the dotted line). This justifies our use of M as a reasonable good esti-

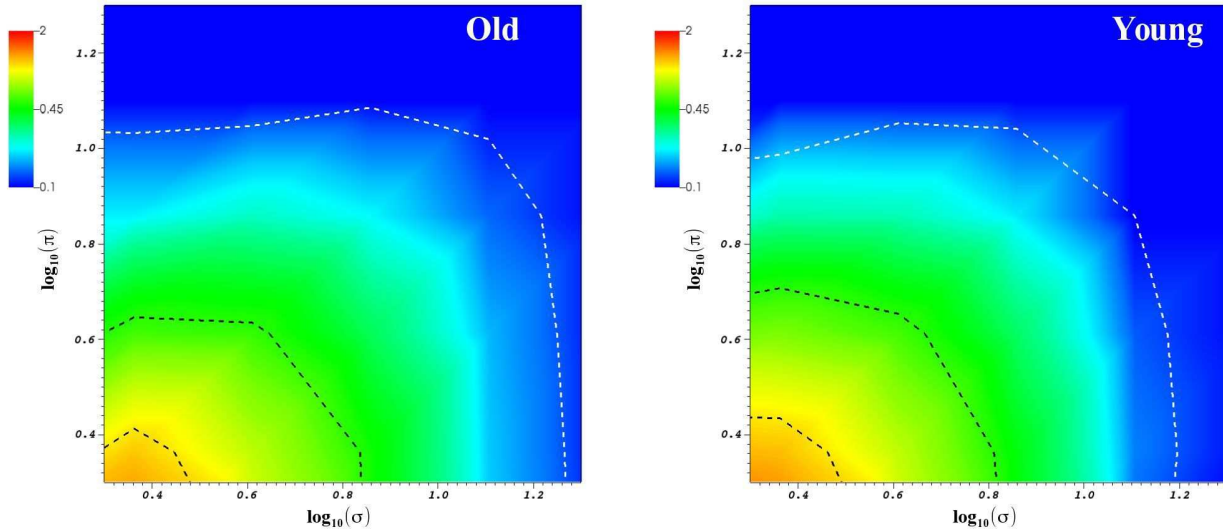


Figure 8. Same as Fig. 2 also for SDSS central galaxies, but using the proxy for peak height defined by the best fitting parameters $a = 0.3$ and $b = -1.08$ in equation (4) in the total mass bin $10^{11.63} < M/h^{-1} M_{\odot} < 10^{12.74}$.

mator of the original peak that gave origin to each central galaxy with the best-fitting values $a = 0.3$ and $b = -0.6$ in the case of the mock catalogue.

In the next section we apply the approach to redefine the overdensity peak height of SDSS galaxies.

4.2 SDSS galaxies

Similarly to the previous Section, we split the samples into three total mass bins in $\log(M/h^{-1} M_{\odot})$ with the same width. We select subsamples that contain the same number of old and young SDSS galaxies for a given mass bin, with the condition $|\delta_t| > 0.5$, but using the distribution of the luminosity-weighted stellar age as a function of the total mass M . Recall this mass is estimated inside a cylinder of radius r . The correlation functions are obtained in redshift space, $\xi(\sigma, \pi)$, and we estimate their projected counterpart as described in Section 3.

For the SDSS central galaxies, the best-fitting values are $a = 0.3$, $b = -1.08$ ($\chi^2 \sim 12.35$). The marginalized probability distributions for a and b are shown as solid lines in Fig. 7, and as can be seen there is a reasonable good agreement with the distributions obtained from our mock catalogue. The correlation functions in redshift space and the projected correlation functions are shown in Figs. 8 and 9, respectively, for the lowest mass bin using these values. Again, the effect of assembly bias is reduced using the proxy for the overdensity peak height at scales $> 1 h^{-1}$ Mpc; for the lowest mass bin the average differences in clustering amplitude are 8 ± 10 per cent in the case of $\omega(\sigma)$. We confirm that our approach is able to define an initial peak-height proxy using the crowding of the region where galaxies lie, in a similar manner to that implemented in Paper I, and that SDSS galaxies show a similar behaviour to mock galaxies since their best-fitting sets of parameters are comparable.

In this context, as mentioned above, Fig. 7 shows

the marginalized likelihood distributions for the free parameters a and b of equation (4) for the SDSS and mock catalogues. By estimating a weighted average for the values in the range of 1σ for the two distributions, we obtain

$$a = 0.26 \pm 0.19$$

$$b = -0.75 \pm 0.36.$$

The best estimates for the a parameter are always positive, whereas those for the b parameter are negative when defining an overdensity peak height proxy using discrete masses. The next section will discuss the properties of this proxy of peaks.

5 PEAKS DEFINED USING DISCRETE MASSES

The redefinition of the overdensity peak height using halo masses within cylinders is able to trace the assembly bias (Section 4). Table 1 shows the median radius of equation (4) in physical units of h^{-1} kpc for three different bins in M_h using the mock central galaxies. The results are shown for the best-fitting values $a = 0.3$, $b = -0.6$. The radius of the cylinder for all the mock central galaxies decreases to higher masses. This is in agreement to what was discussed in Paper I, where the radius decreases to more massive objects. Bear in mind that the radius can be negative, $r < 0$, since both the first and second term of equation (4) can be negative, which implies $M = M_h$. The results are also split according to the classification of old and young populations after performing the redefinition of mass for these mock central galaxies. As in Paper I, old objects have higher radii than young objects of equal mass M_h , thus suggesting stronger environmental dependences for old populations.

Table 2 shows the median radius of equation (4) using the SDSS central galaxies. In general, there is a good agree-

Table 1. Median radii in physical units (h^{-1} kpc) from equation (4) for mock central galaxies (see details in Section 4.1), as given by the best-fitting parameters $a = 0.3$, $b = -0.6$. The results are shown for all mock centrals and, also, split among the old and young populations after performing the redefinition of mass. The radius $r < 0$ implies $M = M_h$. The halo mass M_h is in units of $h^{-1} M_\odot$.

Mock: best-fitting parameters	Ages	$\langle r/h^{-1}\text{kpc} \rangle$	$\langle r/h^{-1}\text{kpc} \rangle$	$\langle r/h^{-1}\text{kpc} \rangle$
$a = 0.3, b = -0.6$		$\log M_h = (12, 12.6)$	$\log M_h = (13, 13.6)$	$\log M_h = (14, 14.6)$
	All	700.0	111.3	< 0
	Old	845.9	273.9	< 0
	Young	371.0	< 0	< 0

Table 2. Median radii in physical units (h^{-1} kpc) from equation (4) for SDSS central galaxies (see details in Section 4.2), as given by the best-fitting parameters $a = 0.3$, $b = -1.08$. The results are shown for all SDSS centrals and, also, split among the old and young populations after performing the redefinition of mass. The radius $r < 0$ implies $M = M_h$. The halo mass M_h is in units of $h^{-1} M_\odot$.

SDSS: best-fitting parameters	Ages	$\langle r/h^{-1}\text{kpc} \rangle$	$\langle r/h^{-1}\text{kpc} \rangle$	$\langle r/h^{-1}\text{kpc} \rangle$
$a = 0.3, b = -1.08$		$\log M_h = (12, 12.6)$	$\log M_h = (13, 13.6)$	$\log M_h = (14, 14.6)$
	All	1231.8	177.8	< 0
	Old	1465.1	376.2	< 0
	Young	971.2	< 0	< 0

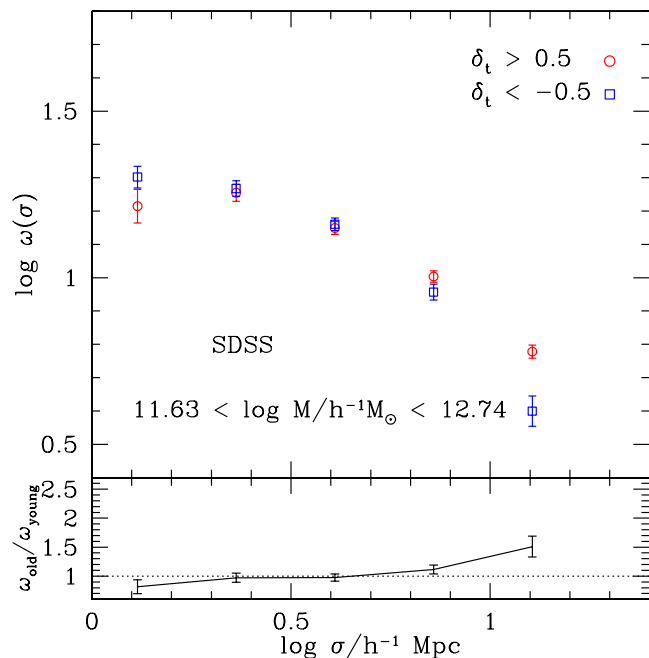


Figure 9. Projected cross-correlation functions for SDSS central galaxies, but with the new proxy mass M by using the best-fitting values $a = 0.3$ and $b = -1.08$. The mass range is indicated in the panel. Old and young SDSS galaxies are shown in red circles and blue squares, respectively. Error bars are calculated using the jackknife method.

ment of the radius sizes with respect to the mock catalogue (see Table 1) for the massive haloes ($M_h > 10^{13} h^{-1} M_\odot$), with differences among them smaller than $102 h^{-1}$ kpc, but the radius for less massive host haloes ($M_h \sim 10^{12.3} h^{-1} M_\odot$) in the case of SDSS galaxies is $\sim 600 h^{-1}$ kpc higher than the radius in the case of mock galaxies of equal host

halo mass. This means that the best-fitting set of parameters that make the assembly bias very low for both mock and real galaxies are somewhat similar when using discrete masses in cylinders as a proxy of peak height, although with the need of higher radius for SDSS galaxies in relatively low-mass host haloes. One reason for this might be related with the fact that, in general, semi-analytic models do not reproduce all the phenomenology of real galaxies (e.g. mass downsizing). However, note that the radius r in equation (4) is strongly determined by the free parameters a and b . Therefore, the differences in the radii reported in Tables 1 and 2 are mainly due to the fact that the best-fitting value is $b = -0.6$ for mock galaxies and $b = -1.08$ for SDSS galaxies. Given the uncertainties (e.g. Fig. 7), it is premature to infer any physical interpretation in this regard.

The method followed to redefine the peak height could be compared to adding up the mass from the smooth density field beyond the virial radius. First, we compare the resulting M mass function in the mock catalogue with the original mass function of haloes with mass M_h to help interpret the changes introduced by our approach; this is equivalent to our procedure in Paper I where we compared the mass functions for the original virial mass, and that resulting from our redefinition of peak height. Fig. 10 shows differences in the mass function that results from the redefinition of mass M for mock central galaxies (solid circles) and that from the host halo mass M_h (open circles). Recall we only use host haloes of central galaxies with the conditions $M_r - 5 \log(h) \leq -19.6$ and $0.01 \leq z \leq 0.1$. One could have expected the number of these objects with mass M to be similar to that of all haloes of mass M_h . The difference between the mass functions measured with M and M_h is relatively small but not negligible. In the next section we will study the origin of this discrepancy.

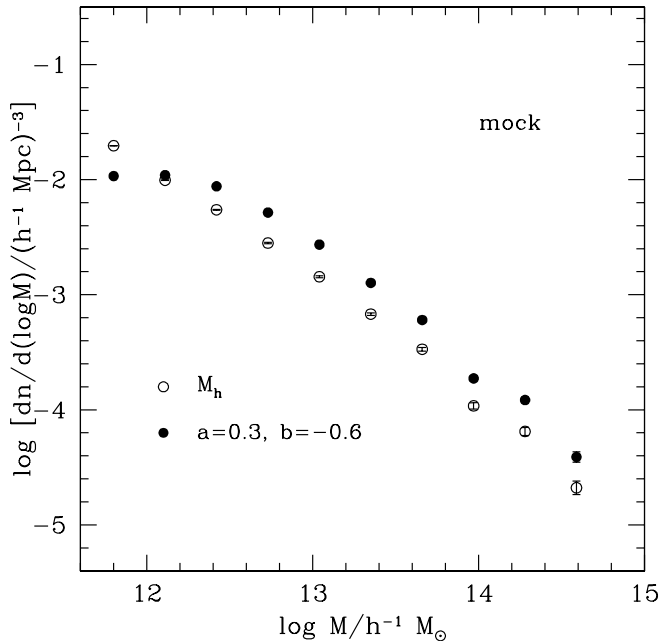


Figure 10. Mass function using the parameters $a = 0.3$ and $b = -0.6$ (solid circles) in the mock catalogue. Open circles correspond to the mass function using the original host halo mass, M_h .

5.1 Discrete mass tracers compared to underlying smooth density field

In Paper I we found that the redefinition based on the mass density field does not change the halo mass function at $M > 10^{12} h^{-1} M_\odot$ (see their Fig. 8) when compared to that obtained from the virial mass. This is in agreement with the result found by Gao et al. (2005) where the assembly bias with respect to formation time is not important for the high mass regime. The reason for the change found in the low-mass regime is that the peak for an old, low-mass object adds more haloes and mass than for a young object of equal mass.

The discrete formalism presented in Section 4 actually measures the crowding around objects which constitutes a different proxy of the peak height than the total underlying mass. In order to compare both proxies of the peak height, we use the semi-analytical galaxies that were used to construct the mock catalogue (see Section 2.2). The discrete mass proxy is performed by means of the total mass of neighbour host haloes within cylinders around synthetic central galaxies with the condition $M_r - 5 \log(h) \leq -19.6$. Only neighbour host haloes with masses $> 10^{11.6} h^{-1} M_\odot$ are considered. On the other hand, the underlying mass proxy is estimated by using the DM particles of the numerical simulation (Section 2.2) contained in spheres around the same synthetic central galaxies. In both cases, the radius of the cylinders/spheres is given by the equation (4). The length of each cylinder is $\Delta v = \pm 500 \text{ km s}^{-1}$ centred at synthetic central galaxies by using the z -axis of the simulation as the line-of-sight and turn the z -coordinate into a recession velocity, $v'_z = 100z + v_z$, where v_z is the velocity component in the z -coordinate. We then repeat the procedure described in Section 4.1, but using cross-correlation functions in real

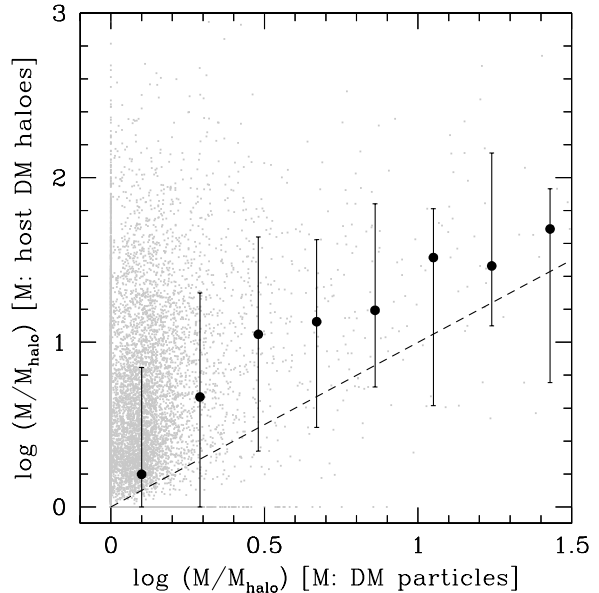


Figure 11. Estimates of the overdensity peak height proxy in Section 5.1 using the approach that considers the mass of DM particles (best-fitting set of parameters $a = 0.3$ and $b = -0.12$, x-axis), and the mass of host DM haloes ($a = 0.1$ and $b = -0.84$, y-axis). This is the total mass contained in spheres and cylinders, respectively, around the same synthetic central galaxies (grey dotted points) in units of the virial mass of their host DM haloes. Solid circles are the medians and the error bars correspond to the 16 and 84 percentiles of the distribution. The dashed line represents a one-to-one relation for both masses.

space in equation (5). The best-fitting parameters obtained for the discrete mass proxy are $a = 0.1, b = -0.84$, which are consistent with the marginalized likelihood functions of the mock catalogue (Fig. 7). The best-fitting values for the underlying mass proxy are $a = 0.3, b = -0.12$. Fig. 11 shows a comparison between the two estimates of the overdensity peak height proxy. The approach that considers the mass of host DM haloes adds on average more mass than the approach using the mass of DM particles, which results in a different mass function (c.f. Fig. 10). However, there is a clear correlation between both methods, indicating that the same phenomenon is being described. We calculate a correlation coefficient using the Pearson's product-moment coefficient,

$$C = \frac{\sum_{i=1}^N (\Delta d_i - \overline{\Delta d})(\Delta u_i - \overline{\Delta u})}{\sqrt{\sum_{i=1}^N (\Delta d_i - \overline{\Delta d})^2} \sqrt{\sum_{i=1}^N (\Delta u_i - \overline{\Delta u})^2}}, \quad (6)$$

where $\Delta d = \log(M/M_h)$ for the discrete mass proxy (y-axis of Fig. 11) and $\Delta u = \log(M/M_h)$ for the underlying mass proxy (x-axis of Fig. 11). Their respective averages are $\overline{\Delta d}$ and $\overline{\Delta u}$. We obtain $C = 0.36$, which means that there is a medium strength in the correlation between both proxies of the peak height, at least with a lower halo mass limit $M_h = 10^{11.6} h^{-1} M_\odot$. This strength in the correlation does

not change if we include in the discrete proxy a scatter in the halo mass of the simulation similar to that found by Y07.

We conclude that although our discrete proxy to measure the total mass will not reproduce the mass function, the reason for this is only the use of discrete neighbours. If we were able to measure the distribution of mass around central galaxies, we would obtain a more physical mass function (e.g. Paper I). This result implies that the phenomena behind the assembly bias, namely, the truncation of infall mass in haloes of low mass embedded in high density regions, can be detected with this discrete proxy for the peak height that can be applied to real galaxy surveys.

6 CONCLUSIONS

We have shown that the assembly bias effect, namely, the difference in the clustering amplitude at large scales of populations of equal mass but different age, exists for both mock central galaxies and SDSS central galaxies. This is a relevant issue that could affect the ability of the next generation of galaxy surveys to infer accurate cosmological parameters. By means of a large halo-based galaxy group catalogue (Y07), constructed from the SDSS, we select central galaxies (i.e. the most massive galaxy in the group). This catalogue includes the estimation of the host halo mass with a lower limit of $M_h = 10^{11.6} h^{-1} M_\odot$. Using the projected correlation function, the clustering strength of old (mock) SDSS central galaxies is (35–55 per cent) 50–70 per cent higher than that of young (mock) SDSS central galaxies of same halo mass ($M_h \sim 10^{11.8} h^{-1} M_\odot$) at projected scales $> 1 h^{-1}$ Mpc. The estimator of age is based on the mass- and luminosity-weighted stellar ages for the synthetic and SDSS galaxies, respectively.

Lacerna & Padilla (2011, Paper I) presented an overdensity peak height proxy with the aim to understand the assembly bias effect. This new definition was proposed as a better alternative than the virial mass. In this work we adapt this model to observations. As the SDSS catalogue is limited in flux, and as the tracers of mass are the host haloes of neighbours central galaxies, the method is modified to use the crowding of the environment around central galaxies, instead of searching for a correction to the virial mass as was done in Paper I. We measure the total mass given by the mass of neighbour host haloes in cylinders centred at each central galaxy, thus obtaining an estimate of the crowding around them, which traces the assembly bias. The radius of this cylinder is parametrized as a function of stellar age and host halo mass of the central galaxy. The best-fitting sets of parameters in the mock catalogue and observations are similar ($a = 0.3$, $b = -0.6$ and $a = 0.3$, $b = -1.08$, respectively). In both cases the assembly bias is lower than 5–15 per cent after using this approach. By estimating a weighted average for the values in the range of 1σ for mock and SDSS central galaxies, it is obtained that the set of best-fitting parameters for the radius of the cylinder is $a = 0.26 \pm 0.19$, $b = -0.75 \pm 0.36$.

This latter model, which constitutes a discrete formalism when counting neighbour haloes within cylinders, does not reproduce the original mass functions since it actually measures the crowding around central galaxies. However, it is reasonably correlated with the smooth density field ap-

proach of Paper I. Therefore, both formalisms help us reach the same conclusion, that the virial mass of dark matter halos sometimes is not appropriate as a proxy for the peak height. It is likely that low-mass haloes in high density environments show their growth truncated by the gravitational effects of their massive neighbours. Our results indicate that this phenomenon also affects the growth of galaxies in addition to the growth of their host dark matter haloes. This might induce a misclassification of galaxies in theoretical models to populate haloes, such as the Halo Occupation Distribution (HOD), because of using virial mass instead of proper peak height.

These results will be of high importance for the next generation of galaxy surveys, such as LSST. The huge amount of information available will allow us to measure the clustering amplitude of galaxies with significant statistics at Mpc scales. Therefore, as we show in this paper, it will be absolutely necessary to model the effect of the environment on the two-halo regime in order to understand its role in the formation and evolution of haloes and galaxies. Theoretical models will have to include this phenomenon in order to reproduce the observational data with high accuracy in the new era of precision cosmology.

ACKNOWLEDGMENTS

We would like to thank Vladimir Avila-Reese for comments and discussions. IL acknowledges support from the Postdoctoral Fellowship program of DGAPA-UNAM, Mexico. NP acknowledges support from Fondecyt No. 1110328, BASAL PFB-06 ‘‘Centro de Astrofísica y Tecnologías Afines’’. FS is supported by the DFG Research Unit FOR 1254. Part of these calculations were performed using the Geryon cluster at AIUC, which received joint funding from Anillo ACT-86, FONDEQUIP AIC-57, and QUIMAL 130008.

REFERENCES

- Adelman-McCarthy J. K., Agüeros M. A., Allam S. S., Anderson K. S. J., et al., 2006, *ApJS*, 162, 38
- Alonso S., Mesa V., Padilla N., Lambas D. G., 2012, *A&A*, 539, A46
- Berlind A. A., Weinberg D. H., 2002, *ApJ*, 575, 587
- Berrier H. D., Barton E. J., Berrier J. C., Bullock J. S., Zentner A. R., Wechsler R. H., 2011, *ApJ*, 726, 1
- Blanton M. R. et al., 2005, *AJ*, 129, 2562
- Cabr e A., Fosalba P., Gazta naga E., Manera M., 2007, *MNRAS*, 381, 1347
- Colless M., Dalton G., Maddox S., Sutherland W., Norberg P., Cole S., Bland-Hawthorn J., et al., 2001, *MNRAS*, 328, 1039
- Cooper M. C., Gallazzi A., Newman J. A., Yan R., 2010, *MNRAS*, 402, 1942
- Cora S. A., 2006, *MNRAS*, 368, 1540
- Croton D. J., Gao L., White S. D. M., 2007, *MNRAS*, 374, 1303
- Dalal N., White M., Bond J. R., Shirokov A., 2008, *ApJ*, 687, 12
- Davis M., Efstathiou G., Frenk C. S., White S. D. M., 1985, *ApJ*, 292, 371

- Faltenbacher A., White S. D. M., 2010, *ApJ*, 708, 469
- Gallazzi A., Charlot S., Brinchmann J., White S. D. M., Tremonti C. A., 2005, *MNRAS*, 362, 41
- Gao L., White S. D. M., 2007, *MNRAS*, 377, L5
- Gao L., Springel V., White S. D. M., 2005, *MNRAS*, 363, L66
- Hahn O., Porciani C., Dekel A., Carollo C. M., 2009, *MNRAS*, 398, 1742
- Hearin A. P., Watson D. F., van den Bosch F. C., 2014, *ArXiv e-prints*
- Kauffmann G., Li C., Zhang W., Weinmann S., 2013, *MNRAS*, 430, 1447
- Lacerna I., Padilla N., 2011, *MNRAS*, 412, 1283
- Lacerna I., Padilla N., 2012, *MNRAS*, 426, L26
- Lagos C. D. P., Cora S. A., Padilla N. D., 2008, *MNRAS*, 388, 587
- Li R., Gao L., Xie L., Guo Q., 2013, *MNRAS*, 435, 3592
- Norberg P., Baugh C. M., Gaztañaga E., Croton D. J., 2009, *MNRAS*, 396, 19
- Skibba R., Sheth R. K., Connolly A. J., Scranton R., 2006, *MNRAS*, 369, 68
- Skibba R. A., Sheth R. K., 2009, *MNRAS*, 392, 1080
- Springel V., White S. D. M., Tormen G., Kauffmann G., 2001, *MNRAS*, 328, 726
- Tinker J., Wetzel A., Conroy C., 2011, *ArXiv e-prints*
- van Daalen M. P., Angulo R. E., White S. D. M., 2012, *MNRAS*, 424, 2954
- Wang H. Y., Mo H. J., Jing Y. P., 2007, *MNRAS*, 375, 633
- Wang L., De Lucia G., Weinmann S. M., 2013a, *MNRAS*, 431, 600
- Wang L., Weinmann S. M., De Lucia G., Yang X., 2013b, *MNRAS*, 433, 515
- Wang Y., Yang X., Mo H. J., van den Bosch F. C., Weinmann S. M., Chu Y., 2008, *ApJ*, 687, 919
- Wechsler R. H., Zentner A. R., Bullock J. S., Kravtsov A. V., Allgood B., 2006, *ApJ*, 652, 71
- Wu H. Y., Rozo E., Wechsler R. H., 2008, *ApJ*, 688, 729
- Xie L., Gao L., Guo Q., 2014, *MNRAS*, 441, 933
- Yang X., Mo H. J., van den Bosch F. C., 2003, *MNRAS*, 339, 1057
- Yang X., Mo H. J., van den Bosch F. C., 2006, *ApJL*, 638, L55
- Yang X., Mo H. J., van den Bosch F. C., Pasquali A., Li C., Barden M., 2007, *ApJ*, 671, 153
- Yang X., Mo H. J., van den Bosch F. C., 2008, *ApJ*, 676, 248
- York D. G., Adelman J., Anderson Jr. J. E., Anderson S. F., Annis J., et al., 2000, *AJ*, 120, 1579
- Zapata T., Perez J., Padilla N., Tissera P., 2009, *MNRAS*, 394, 2229
- Zehavi I. et al., 2002, *ApJ*, 571, 172
- Zentner A. R., Hearin A. P., van den Bosch F. C., 2013, *ArXiv e-prints*
- Zhu G., Zheng Z., Lin W. P., Jing Y. P., Kang X., Gao L., 2006, *ApJL*, 639, L5